scientific reports

OPEN

Numerical simulation for MHD Oldroyd-B fluid flow with melting and slip effect

Amit Dadheech[1], Surbhi Sharma[1] & Qasem Al-Mdallal[2✉]

This investigation reflects an examination of Oldroyd-B fluid flow over a permeable surface subjected to the effects of melting, slip effect, inclined magnetic field and chemical reactions. The governing equations are resolved using the bvp4c inbuilt MATLAB tool, the arithmetic computation for the momentum, thermal and concentration equations are executed. The results are exhibited graphically. Numerical outcomes are graphically depicted by aid of velocity, concentration, temperature profiles for several model variables. The achieved results exhibit a promising agreement with the previously established findings available in the open literature. The results obtained indicated that Deborah number β_1 reduces the momentum boundary layer thickness whereas Deborah number β_2 enhances the adjacent momentum boundary layer. Furthermore, temperature profile declined for melting parameter Me. The application of this study transcends various engineering disciplines, offering practical solutions and optimization opportunities in polymer processing, coating technologies, cooling systems, materials processing, biomedical and environmental engineering.

Keywords Oldroyd-B fluid, Slip effect, Chemical reaction, Non-linear radiation

List of symbols

b	Constant parameter
B_0	Strength of magnetic field ($\text{kgs}^{-2}\text{A}^{-1}$)
C	Fluid's concentration (kgm^{-3})
C_f	Skin friction coefficient
C_p	Specific heat ($\text{J kg}^{-1}\text{ k}^{-1}$)
C_w	Fluid concentration at the wall (kgm^{-3})
D_m	Coefficient of mass diffusion (m^2s^{-1})
Ec	Eckert number
κ	Thermal conductivity (W/m K)
k^*	Mean absorption coefficient
K_n	Chemical reaction parameter
L_1	Velocity slip factor
L_2, L_3	Temperature and Mass slip factor
K_p	Porous parameter
M	Magnetic field parameter
Me	Melting parameter
Nu_x	Local Nusselt number
Pr	Prandtl number
$q_w(x)$	Local surface heat flux (W m^{-2})
q_r	Radiative heat flux
q^*	Heat generation or absorption
Re_w	Local Reynolds number
R	Radiation parameter
A^*, B^*	Space dependent parameter
S	Section/injection parameter
Sh_x	Sherwood number

[1]Department of Mathematics, Swami Keshvanand Institute of Technology, Management & Gramothan, Jaipur, India. [2]Department of Mathematical Sciences, UAE University, P.O. Box 15551, Al Ain, Abu Dhabi, United Arab Emirates. ✉email: q.almdallal@uaeu.ac.ae

nature portfolio

1

T_0	Solid surface temperature (K)
T_∞	Free stream temperature (K)
u_w	Surface velocity (ms^{-1})
u, v	Velocity component corresponding to horizontal and the vertical direction (ms^{-1})
ρ	Fluid density (kgm^{-1})
υ	Kinematic viscosity (m^{2}s^{-1})
σ	Electrical conductivity (sm^{-1})
α	Angle of inclination of magnetic field
λ_1	Relaxation times
λ_2	Retardation times
δ_1	Velocity slip
δ_2	Temperature slip
δ_3	Mass slip
β_1	Deborah number in relaxation time
β_2	Deborah number in retardation time
θ_w	Temperature ratio parameter
$f'(\eta)$	Non-dimensional velocity parameter
$\theta(\eta)$	Non-dimensional temperature parameter
BL	Boundary layer
$\phi(\eta)$	Non-dimensional concentration parameter

Viscoelastic fluids, characterised by their combined elastic and viscous properties, have been the subject of extensive research across multiple scientific and engineering disciplines. Understanding their flow behavior is of paramount importance in numerous applications, such as polymer processing, food manufacturing, biomedical engineering, and oil industry operations. Among the various viscoelastic fluid, the Oldroyd-B fluid model stands out as a widely recognised and extensively studied model, offering insights into the unique characteristics of these complex fluids. Oldroyd-B model[1] is defined by a constant-viscosity, incorporating both relaxation time and retardation time in its formulation. Hayat et al.[2] illustrated the MHD BL flow for an Oldroyd-B fluid within a porous channel featuring suction/injection characteristics. Fetecau et al.[3] suggested an unsteady flow of Oldroyd-B fluid over a plate. Tan et al.[4] extended Stoke's first problem for the Oldroyd-B fluid within a porous medium, and they provided a precise solution by employing the Fourier Sine transform. Goyal and Sharma[5] investigated the behavior of an Oldroyd-B fluid caused by an exponentially extending sheet, considering the influences of radiation and heat section/injection. Khan et al.[6] explored the impact of heat generation 2D radiative effects on the flow of nanofluid caused by a nonlinearly stretchy surface with micro-organisms.

Studying the phenomenon of fluid flow and heat transfer in the presence of magnetic fields, known as magnetohydrodynamics (MHD), has gained significant attention due to its relevance in numerous scientific and engineering applications. In MHD boundary layer flow, a magnetic field applies a force to the charged particles present in the fluid, and this force has the potential to alter the fluid velocity, leading to the generation of vortices and turbulence. One particular problem that has received considerable interest is the MHD flow past a stretching sheet. This configuration represents a simplified model for a variety of practical situations, such as polymer processing, metal production, and boundary layer flows over solid surfaces. Numerous studies and advancements have emerged, contributing to a better understanding of fluid behavior in the presence of a magnetic field, as indicated by references[7-9].

Heat transfer is a fundamental phenomenon that plays a crucial role in various fluid flow processes and engineering applications. Understanding and controlling heat transfer in fluid flows is essential for optimizing system performance, improving energy efficiency, and ensuring the reliability and safety of industrial processes. Fluid flow encompasses a wide range of applications including, but not limited to, thermal power generation, chemical processes, HVAC systems, and transportation. In these systems, heat transfer occurs through conduction, convection, and radiation, depending on the characteristics of the fluid, the surrounding environment, and the heat source or sink. Christov[10] enhanced the model originally introduced by Maxwell–Cattaneo by reintroducing the partial derivative feature. As a result, the model that surfaced is widely acknowledged as the Cattaneo–Christov heat-flux model. In a study by Hosseinzadeh[11], the flow of Maxwell fluid caused by a porous medium was examined, revealing that the Prandtl number exerts substantial influence on both the heat transfer coefficient and the fluid temperature. Gholinia et al.[12] investigated the impact of thermal radiation on the flow of various nanofluids around a vertical cylinder. They noted that the fluid temperature increases due to the higher thermal conductivity of nanoparticles. Hashim et al.[13] conducted a study on the hydro-magnetic nanofluid flow induced by a continuously enlarging sheet under convective boundary conditions at the sheet's surface.

The study of heat transfer during the melting process over stretched sheets represents a critical intersection of thermodynamics and fluid dynamics. The interaction between a solid surface and a moving fluid, coupled with the energy exchange accompanying the phase transition from solid to liquid, gives rise to a myriad of thermal complexities. Understanding the intricacies of melting heat transfer over a stretched sheet is crucial for optimising numerous industrial processes, such as polymer processing, crystal growth, and metal casting. Singh et al.[14] explored the influence of melting-heat transport in the stagnation point flow of magnetohydrodynamic micro-polar fluid approaching a stretching sheet, employing carbon nanotubes in their investigation. Hayat et al.[15] conducted a numerical examination to investigate the effects of melting heat transport and homogeneous-heterogeneous reactions in a flowing system. Following that, Epstein et al.[16] and Ishak et al.[17] inspected the melting-heat transfer in continuous laminar flow past a plate and a moving surface, respectively. Within a micropolar fluid context, Yacob et al.[18] explored heat transfer in the BL stagnation-point flow toward a

stretching sheet, incorporating the melting effect. Olkha et al.[19] deliberated entropy analysis for the MHD flow over a stretchy sheet along with melting phenomena. Dadheech et al.[20] studied MHD flow across a stretching surface for Casson fluid in the presence of melting and slip-effects. Dadheech et al.[21] deliberated entropy optimization for the non-Newtonian fluid over a vertical plate along with Cattaneo-Christov heat flux and slip effect.

The slip effect, which allows for relative motion between the fluid and the solid surface, introduces a layer of complexity that significantly influences the overall behavior of the system. This condition has been recognized as a crucial factor in various engineering scenarios, including polymer processing, coating applications, and aerodynamics. The impact of slip-on fluid dynamics becomes particularly pronounced when studying the stretching sheet phenomenon, as the interplay between fluid flow and surface deformation can lead to fascinating and often counterintuitive outcomes. Labropulu et al.[22] discoursed the effects of slip BC (boundary condition) for non-Newtonian fluid flows. Ali et al.[23] examined slip phenomena in non-Newtonian viscoelastic fluid flow owing to oscillatory continuous stretched surface. Govindarajan et al.[24] deliberated slip, mass-transport phenomena in a vertical channel in light of radiation. Dawar et al.[25] investigated slip flow of a Maxwell fluid induced by a stretchable surface in non-linearly manner. Furthermore, it is noteworthy to mention that similar investigations have been conducted and documented in previous studies[26–41], which are relevant to the current context.

The primary purpose of this study is to explore the flow behavior of an MHD Oldroyd-B fluid and its heat transfer characteristics over a stretching sheet, accounting for the presence of melting and slip effects, which have not been adequately explored in existing literature. Moreover, the study is observed in the presence of a porous medium, including melting and slip effects, adding novelty to our investigation. Significant implications of the showcased demonstration are outlined for application in engineering setups and the effective improvement of systems involving thermo-fluid flow, polymer processing, and similar domains. Various results related to physical parameters are explicitly explained.

Mathematical formulation

Here we considered a steady-state boundary layer flow, as well as heat and mass transfer, involving an incompressible Oldroyd-B fluid flow within a porous medium over a permeable surface, as illustrated in Fig. 1. The surface under consideration is undergoing linear stretching along the x-direction with a velocity that is described by $u_w = bx$, taking $b > 0$.

The governing system of equations for Oldroyd-B fluid, as proposed by Goyal and Sharma[5], along with their respective boundary conditions (BC), are mentioned below:

$$\frac{\partial u}{\partial x} + \frac{\partial v}{\partial y} = 0 \tag{1}$$

$$u\frac{\partial u}{\partial x} + v\frac{\partial u}{\partial y} + \underbrace{\lambda_1\left(u^2\frac{\partial^2 u}{\partial x^2} + v^2\frac{\partial^2 u}{\partial y^2} + 2uv\frac{\partial^2 u}{\partial x\partial y}\right)}_{Non-newtonian\ term} = \upsilon\frac{\partial^2 u}{\partial y^2}$$

$$+ \underbrace{\lambda_2\upsilon\left(u\frac{\partial^3 u}{\partial x\partial y^2} + v\frac{\partial^3 u}{\partial y^3} - \frac{\partial u}{\partial y}\frac{\partial^2 u}{\partial y^2} - \frac{\partial u}{\partial y}\frac{\partial^2 v}{\partial y^2}\right)}_{Non-newtonian\ term} - \underbrace{\frac{\sigma B_0^2 \sin^2\alpha}{\rho}\left(u + \lambda_1 v\frac{\partial u}{\partial y}\right)}_{Megnetic\ field} - \underbrace{\frac{\upsilon}{k_p}u}_{Porous\ medium\ term} \tag{2}$$

$$u\frac{\partial T}{\partial x} + v\frac{\partial T}{\partial y} = \frac{\kappa}{\rho C_p}\frac{\partial^2 T}{\partial y^2} - \underbrace{\frac{1}{\rho C_p}\frac{\partial q_r}{\partial y}}_{Radiative\ term} + \frac{\sigma B_0^2 \sin^2\alpha}{\rho C_p}u^2 + \underbrace{\frac{q^*}{\rho C_p}}_{Heat\ source} \tag{3}$$
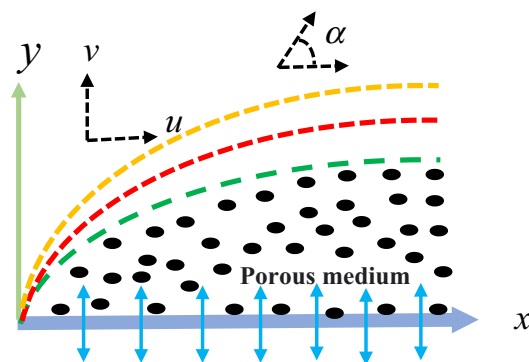

Figure 1. Physical model of the problem.

$$u\frac{\partial C}{\partial x} + v\frac{\partial C}{\partial y} = D_m\frac{\partial^2 C}{\partial y^2} - \underbrace{k_n(C - C_\infty)^n}_{\text{Chemical reaction}} \tag{4}$$

To elucidate the physical parameters, kindly consult the provided nomenclature. A suitable boundary condition for the fluid flow, concentration and temperature (Olkha et al.[7]), is given by:

$$at\ y = 0 \begin{cases} u = \underbrace{u_w + L_1\frac{\partial u}{\partial y}}_{\text{Velocity Slip}}, \quad \underbrace{v = \kappa\frac{1}{\rho\{\beta_m + c_s(T_m - T_0)\}}\frac{\partial T}{\partial x} - v_m,}_{\text{melting term}} \\ \underbrace{T = T_m + L_2\frac{\partial T}{\partial y},}_{\text{Temperature Slip}} \\ \underbrace{C = C_w + L_3\frac{\partial C}{\partial y},}_{\text{Mass Slip}} \end{cases} \tag{5}$$

$$at\ y \to \begin{cases} u \to 0, \\ T \to T_\infty, \\ C \to C_\infty, \end{cases}$$

For radiative heat transfer, Rosseland diffusion flux model is considered. Following Siegel and Howell (1972) it reduces to following form

$$q_r = -\frac{4\sigma_1}{3k^*}\frac{\partial T^4}{\partial y}$$

Here it is supposed that the medium is optically thick and gray; absorbing-emitting, but non-scattering.

We assumed that the temperature variations within the fluid flow are significantly negligible. By expanding T^4 using Taylor's series around T_∞ and neglecting higher order terms, we obtain:

$$T^4 \approx 4T_\infty^3 T - 3T_\infty^4$$

then

$$q_r = \frac{-16\sigma_1 T_\infty^3}{3k^*}\frac{\partial T}{\partial y}$$

Were σ_1 and k^* are the Stefan-Boltzmann constant and the mean absorption coefficient for radiation respectively.

Solution

Implementing the similarity transformations listed below (Goyal et al.[5]):

$$\eta = y\sqrt{\frac{b}{v}}, \quad u = bxf'(\eta), \quad v = -\sqrt{bv}f(\eta),$$
$$\phi(\eta) = \frac{C - C_\infty}{C_w - C_\infty}, \quad \theta(\eta) = \frac{T - T_\infty}{T_m - T_\infty} \tag{6}$$

Continuity equation is identically self-satisfied. Employing Eq. (6) in (2–4) will result in following non-linear ODE's:

$$f''' - f'^2 + f''f + \beta_1\left(2ff'f'' - f^2f'''\right)$$
$$+ \beta_2\left(f''^2 - ff^{iv}\right) - \left\{M\sin^2\alpha\left(f' + \beta_1 ff''\right)\right\} - Kpf' = 0 \tag{7}$$

$$\theta'' + A^*f' + B^*\theta + \frac{4}{3}R\left[\{(\theta_w - 1)\theta + 1\}^3\theta'' + 3(\theta_w - 1)\{(\theta_w - 1)\theta + 1\}^2\theta'^2\right]$$
$$+ \Pr\left(Ec\,M\,\sin^2\alpha f'^2 + f\theta'\right) = 0 \tag{8}$$

$$\phi'' - Sc\left(Kn\phi^n - f\phi'\right) = 0 \tag{9}$$

Transformed B.C. are:
BC

4

$$at \quad \eta = 0 \quad \begin{cases} f'(\eta) = 1 + \delta_1 f''(\eta), \\ \theta(\eta) = 1 + \delta_2 \theta'(\eta), \\ \phi(\eta) = 1 + \delta_3 \phi'(\eta), \\ f(\eta) = S - \frac{Me}{Pr}\theta', \end{cases} \tag{10}$$

$$as \ \eta \to \infty \quad \begin{cases} f'(\eta) \to 0, \\ \theta(\eta) \to 0, \\ \phi(\eta) \to 0, \end{cases}$$

where Magnetic field parameter: $M = \frac{\sigma B_0^2}{\rho b}$, Prandtl number: $Pr = \frac{\mu C_p}{\kappa}$, Schmidt number: $Sc = \upsilon / D_m$, Suction/Injection coefficient: $S = \frac{V_0}{\sqrt{b\upsilon}}$, Porosity parameter: $Kp = \upsilon / bk_p$, Chemical reaction parameter: $Kn = k_n(C_w - C_\infty) / b$, Velocity slip parameter: $\delta_1 = L_1\sqrt{b/\upsilon}$, Melting surface parameter: $Me = \frac{(T_m - T_\infty)C_p}{\beta_m + c_s(T_m - T_0)}$, Temperature slip parameter: $\delta_2 = L_2\sqrt{b/\upsilon}$, Radiation Parameter: $R = 4\sigma_1 T_\infty^3 / \kappa k^*$, Mass slip parameter: $\delta_3 = L_3\sqrt{b/\upsilon}$, $\beta_1 = \lambda_1 c$ and $\beta_2 = \lambda_2 c$ are Deborah number in relaxation and retardation time respectively, $S = v_w / \sqrt{b\upsilon}$: suction/injection parameter.

Methodology

Equations (7–9) are resolved using the bvp4c tool in MATLAB, following the boundary condition specified in (10). Initially, the nonlinear Eqs. (7–10) were expressed as a system of linear equations:

$$f = y_1, f' = y_2, f'' = y_3, f''' = y_4, f'''' = y_4'$$
$$\theta = y_5, \theta' = y_6, \theta'' = y_6'$$
$$\phi = y_7, \phi' = y_8, \phi'' = y_8'$$

$$y_4' = \frac{\begin{cases} y_4 - y_2^2 + y_1 y_3 + \beta_1\left(2y_1 y_2 y_3 - y_1^2 y_4\right) \\ \quad + \beta_2 y_3^2 + \left\{ M\sin^2\alpha\left(y_2 + \beta_1 y_1 y_2\right)\right\} + y_2 Kp \end{cases}}{\beta_2 y_1}$$

$$y_6' = \frac{-\left[A^* y_2 + B^* y_5 + 4R(\theta_w - 1)\{(\theta_w - 1)\theta + 1\}^2 y_6^2 + Pr\left(Ec\, M\,\sin^2\alpha y_2^2 + y_1 y_6\right)\right]}{\left(1 + \frac{4}{3}R\{(\theta_w - 1)\theta + 1\}^3\right)}$$

$$y_8' = Sc\left(Kn\, y_7^n - y_1 y_8\right)$$

BC

$$y_2(0) = 1 + \delta_1 y_3(0), \quad y_1(0) = S - \frac{Me}{Pr}y_6(0), \ y_5(0) = 1 + \delta_2 y_6(0), \quad y_7(0) = 1 + \delta_2 y_7(0)$$
$$y_2(\infty) \to 0, \quad y_5(\infty) \to 0, \quad y_7(\infty) \to 0$$

Physical quantities of interest

The C_f: skin friction coefficient, Nu_x: local Nusselt number, Sh_x: local Sherwood number are given as:

$$C_f = \frac{\tau_w}{\rho u_w^2}; \ Nu_x = \frac{xq_w}{\kappa(T_w - T_\infty)}; \ \text{and} \ Sh_x = \frac{x J_w}{D_m(C_w - C_\infty)} \tag{11}$$

where

$$\tau_w = \mu\left(\frac{\partial u}{\partial y}\right)\Big|_{y=0}, \ \text{wall shearing stress;} \ q_w = -\left(\kappa + \frac{16\sigma_1 T^3}{3k^*}\right)\left(\frac{\partial T}{\partial y}\right)\Big|_{y=0}, \ \text{surface heat flux;}$$
$$J_w = -D_m\left(\frac{\partial C}{\partial y}\right)\Big|_{y=0}, \ \text{surface mass flux} \tag{12}$$

Utilizing Eq. (6) within the context of Eq. (11), the subsequent expressions for skin friction coefficient (C_f), local Nusselt number (Nu_x) and local Sherwood number (Sh_x) are attained:

$$C_f\sqrt{Re_x} = f''(0), \tag{13}$$

$$Nu/\sqrt{Re_x} = -\left[1 + \frac{4R}{3}\{1 + (\theta_w - 1)\theta(0)\}^3\right]\theta'(0), \tag{14}$$

$$Sh/\sqrt{Re_x} = -\phi'(0). \tag{15}$$

$\text{Re}_x = \frac{bx^2}{v}$ is local Reynold number.

Result and discussion

The transfigured governing Eqs. (7–9) mentioned earlier are numerically addressed using bvp4c function, a built-in MATLAB tool, with the boundary conditions specified in Eq. (10). The outcomes thus obtained signify significant implications of non-dimensional governing variables as β_1 and β_2 that represents Deborah number in relaxation and retardation time respectively, M magnetic field parameter, δ_1, δ_2, δ_3 Velocity, temperature and mass slip parameter, Kp porous medium parameter, R radiation parameter, temperature ratio parameter θ_w, Me Melting parameter, Ec Eckert number, Inclined angle α, Sc Schmidt number, parameter of Chemical reaction Kn, non-uniform heat source/sink parameters A^* on velocity, temperature, and concentration profile respectively. Mathematical computations are conducted, and the favourable effects of the parameters involved are investigated concerning the profiles of velocity, temperature, and mass, utilizing relevant graphical data. To validate the current findings, the results are compared with those of Anderson et al.[27], Prasad et al.[28], Khan et al.[29] and Wang[26], which are presented in Tables 1 and 2. The observed concordance with these works is noted as satisfactory and supportive Table 3 show the C_f. Nh_x, Sh_x for various value of the physical parameter.

Figure 2a–c depict consequence of magnetic-field factor (M) on velocity, temperature and concentration profiles respectively. It has been observed that velocity profile goes down by enhancing M (see Fig. 2a). Physically, when a magnetic field is applied to a conducting fluid, it induces an electric current within the fluid. The interaction of this electric current with the magnetic field results in a force referred to as the Lorentz force. As the magnetic field strength increases, Lorentz force becomes more pronounced, creating greater resistance to fluid motion and consequently leading to a reduction in fluid velocity. However, contrasting effects are noticed on the profiles of $\phi(\eta)$, $\theta(\eta)$ (see Fig. 2b,c).

The velocity ($f'(\eta)$), temperature ($\theta(\eta)$), concentration ($\phi(\eta)$) profile are influenced by the porous medium parameter (Kp), as illustrated in Fig. 3a–c. The thickness of temperature and concentration profiles are extended as Kp upsurges while the $f'(\eta)$ profile gets diminished. Figure 3a illustrates that elevating values of Kp results in a reduction in flow velocity. or lessening permeability parameter (k_p). Momentum equation reveals that Darcian resistance force is inversely proportional to the (k_p). Consequently, a low permeability will produce a significant Darcian resistance to fluid flow. Thus, flow-field is observed diminishing as the Kp increases.

Figure 4a–c depict the interesting phenomenon on Deborah number (β_1) on the profiles of velocity, temperature, and mass. The velocity distribution diminutions with growing values of the Deborah number, while the thickness of temperature and mass boundary layers increases. In physical terms, the ratio of relaxation time to observation time is linked to the Deborah number. As an increase in the Deborah number indicates a longer relaxation time, leading to greater resistance to the fluid motion and, consequently, a decrease in the velocity profile. Figure 5a–c are shows $f'(\eta)$, $\theta(\eta)$, $\phi(\eta)$ distribution affected by Deborah number (β_2) (in the terms of retardation time). It has been established that the velocity profile shows notable improvement with higher values of the Deborah number, while the temperature and concentration profiles are observed to decrease.

Impact of Pr, Ec and θ_w on temperature $\theta(\eta)$ profiles are constituted in Fig. 6a-c. It has been concluded that temperature distribution decreases for Pr whereas temperature distribution improves for Ec and θ_w. Impact of Sc and Kn are instituted in Fig. 7a,b on $\phi(\eta)$ profiles. Mass profile decreases with rising values Sc and Kn. Physically, an increase in the Sc demonstrates an enhancement in the momentum diffusivity of the fluid, demonstrating increase rate of mass flow important to fewer mass credits on surface.

Figure 8a,b indicates that concentration profile $\phi(\eta)$ and temperature $\theta(\eta)$ are declined when the physical parameter Me is increased accordingly. Physically, when the melting parameter increases, it implies that the heat generation due to melting becomes more significant. As a result, more heat is generated within the boundary layer close to the sheet surface. This increased heat generation counteracts the convective heat transfer from the fluid flow. Consequently, the temperature profile in the BL decreases as heat generation due to melting dominates the heat transfer process.

Figure 9a–c serve to illustrate the effects δ_1, δ_2 and δ_3 on $f'(\eta)$, $\theta(\eta)$, $\phi(\eta)$ profile. It has been concluded that $f'(\eta)$, $\theta(\eta)$ and $\phi(\eta)$ profiles is commendably declined for higher values of δ_1, δ_2 and δ_3. Physically, as the velocity

Pr	Wang[26]	Khan et al.[29]	Present study
0.7	0.454	0.454	0.4540471
2.0	0.911	0.911	0.9113625

Table 1. Comparison of $-\theta'(0)$ for distinct values of Pr when $\beta_1 = A^* = \beta_2 = S = R = M = B^* = Kn = \alpha = 0$.

M	Anderson et al.[27]	Prasad et al.[28]	Present study
1.0	1.414000	1.414449	1.4142586
1.5	1.581000	1.581139	1.5811481
2.0	1.732000	1.732203	1.7320505

Table 2. Comparison of $-f''(0)$ for distinct values of M when $\beta_1 = \beta_2 = S = R = Ec = \alpha = A^* = B^* = Kn = 0$.

M	Pr	Kp	Me	S	R	β_1	β_2	Cf	$-Nh_x$	$-Sh_x$
3								−2.005549569	0.645206952	1.077520268
6								−2.296626507	0.506509076	1.034232813
9								−2.530221494	0.405747366	1.004277722
	2							−2.000664821	0.330581757	0.978790757
	4							−2.008165049	0.918660005	1.128786293
	6							−2.010855432	1.363926371	1.180321909
		3						−2.005549569	0.645206952	1.077520268
		4						−2.115899795	0.623176740	1.060715986
		5						−2.216728742	0.603089981	1.046201739
			0.02					−1.890180743	0.804089308	1.193364385
			0.04					−1.883386033	0.669357234	1.097208984
			0.06					−1.876809918	0.529722956	1.003258477
				0.1				−1.835850688	0.520687468	1.307160416
				0.3				−1.894672617	0.888273369	1.255930937
				0.5				−1.920321937	1.308675802	1.591665706
					0.1			−1.920321937	1.308675802	1.591665706
					0.2			−1.920318186	1.306584930	1.591619476
					0.3			−1.920314470	1.304514156	1.591573688
						0.4		−1.884458040	1.312659296	1.598132897
						0.6		−1.860668943	1.315236719	1.602552871
						0.8		−1.837154418	1.317709875	1.607029985
							0.5	−1.598228442	1.332055766	1.637200363
							0.7	−1.497316747	1.337037670	1.649842234
							0.9	−1.416447321	1.339893294	1.659941049

Table 3. Show the values of the skin friction coefficient, local Sherwood number and Nusselt number for various parameters.

slip parameter increases, it indicates a larger slip velocity at the fluid–solid interface, where the fluid molecules experience reduced interaction with the solid surface. As a result, the momentum transfer among the fluid and the solid surface weakens, leading to a lessening in the velocity profile.

Figure 10a,b exhibits nature of (β_1) on skin frication (Cf_x) and Nusselt number (Nu_x). It is found that skin frication increases and on the other side Nusselt number decreases for the value of β_1 whereas Fig. 11a,b exhibits consequences of (β_2) on skin frication (Cf_x) and Nusselt number (Nu_x). It is found that (Cf_x) increases whereas (Nu_x) is subside for value of β_2.

Conclusions

The present study offers numerical results for the magnetohydrodynamic flow of an Oldroyd-B fluid over a continuously stretching sheet. The numerical outcomes of the transformed ODE's are presented graphically, allowing for an exploration of the acceptable values of the regulating parameters in the specified problem. The essential outcomes are listed as follows:

- An increase in the porous medium parameter Kp leads to a reduction in the corresponding velocity profile $f'(\eta)$.
- An elevation in the β_1 is associated with a decline in the corresponding thevelocity profile $f'(\eta)$. On the flip side, an enhancement in the Deborah number results in a rise in the temperature profile.
- The velocity profile is positively influenced by the Deborah number β_2, indicating that velocity is an increasing function dependent on the effects of the Deborah number β_2.
- $\theta(\eta)$ profile is decreasing as a functions of corresponding parndtl number Pr.
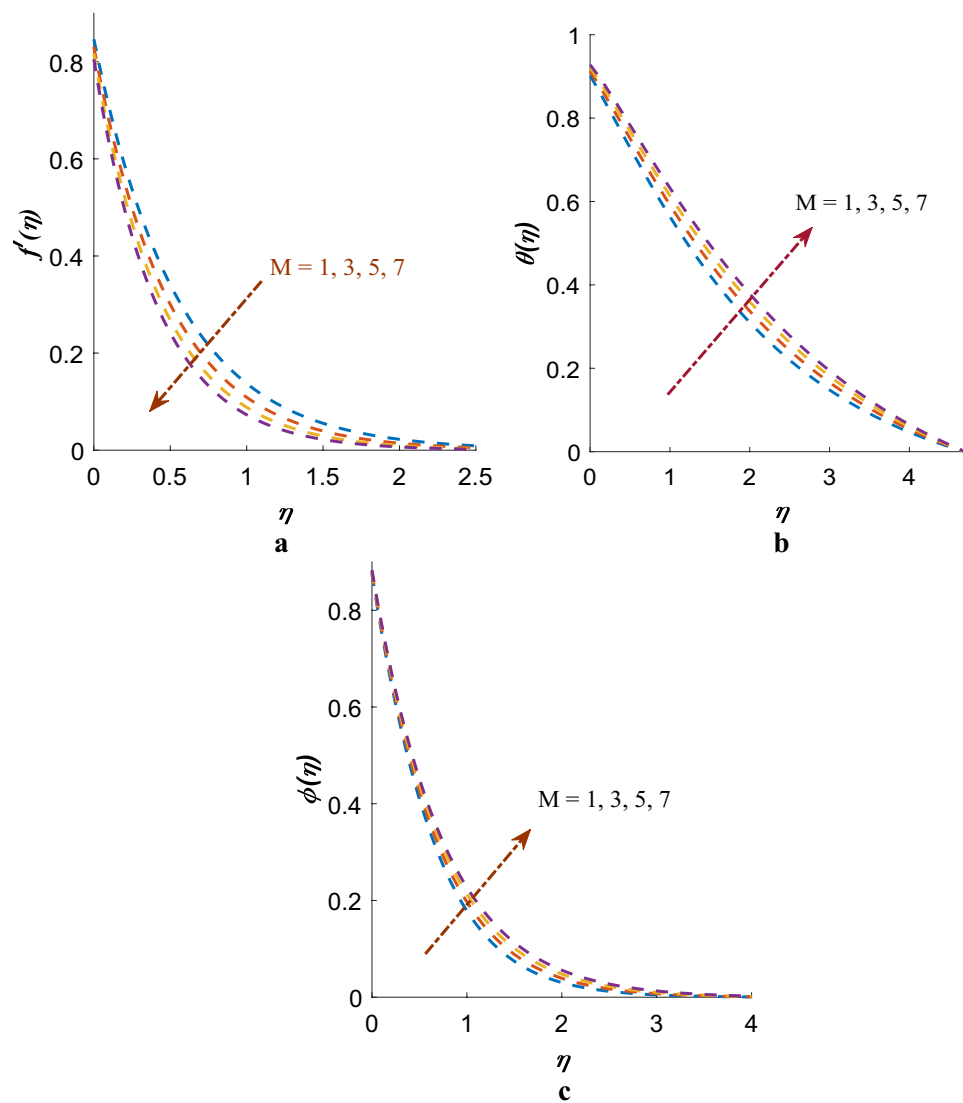- The concentration field diminishes as the corresponding Schmidt number Sc increases.

Figure 2. (**a**) Variation of M on $f'(\eta)$. (**b**) Effect of M on $\theta(\eta)$. (**c**) Variation of M on $\phi(\eta)$.
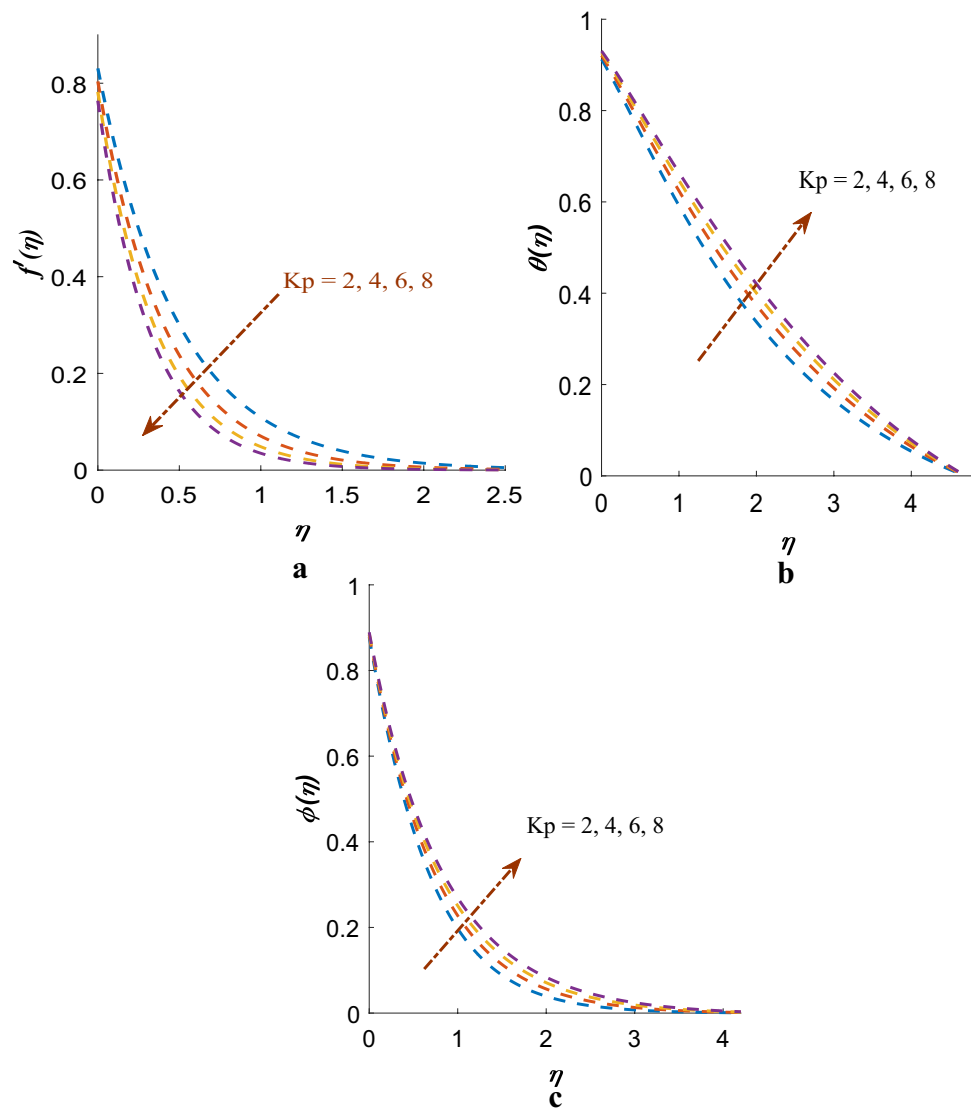
Figure 3. (**a**) Effect of Kp on $f'(\eta)$. (**b**) Effect of Kp on the $\theta(\eta)$. (**c**) Effect of Kp on $\phi(\eta)$.
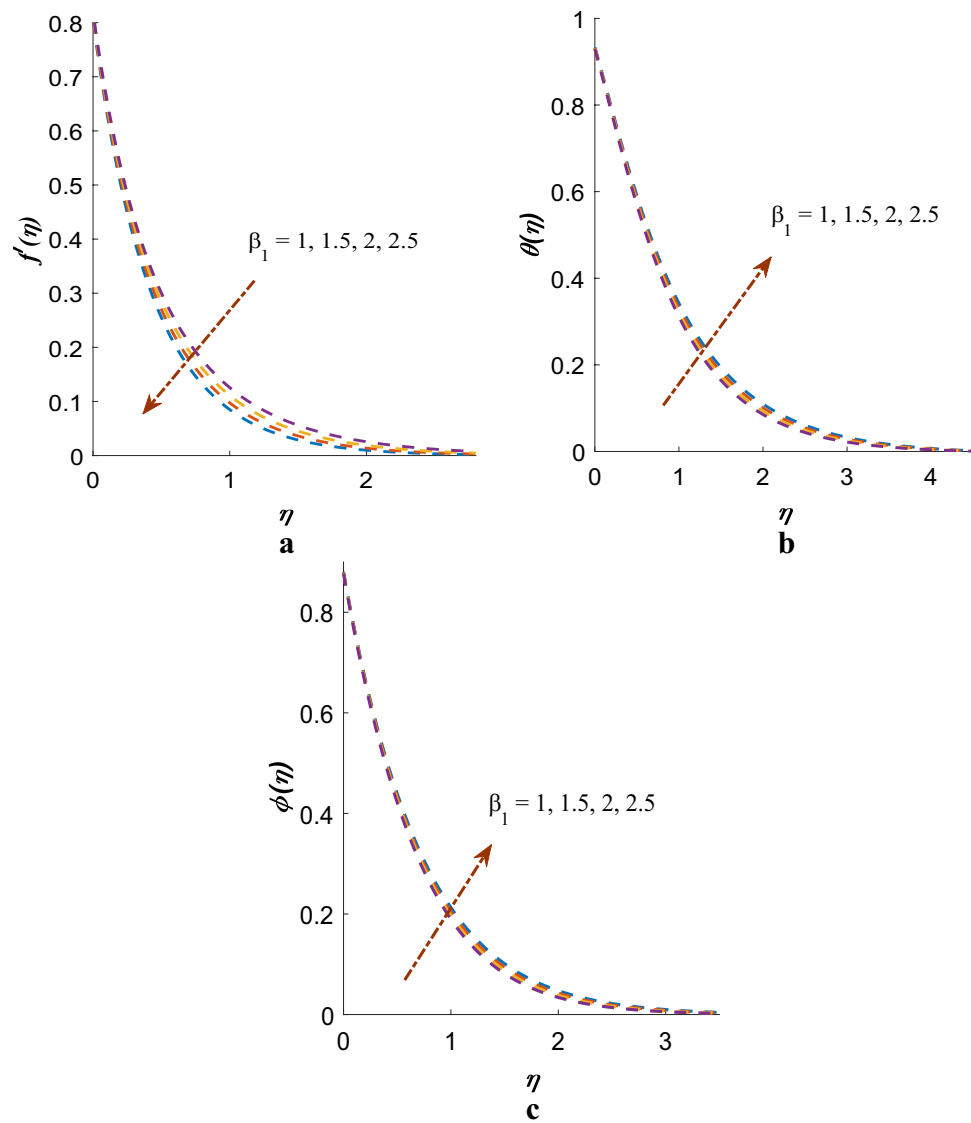
Figure 4. (**a**) Effect of β_1 on $f'(\eta)$. (**b**) Effect of β_1 on $\theta(\eta)$. (**c**) Effect of β_1 on $\phi(\eta)$.
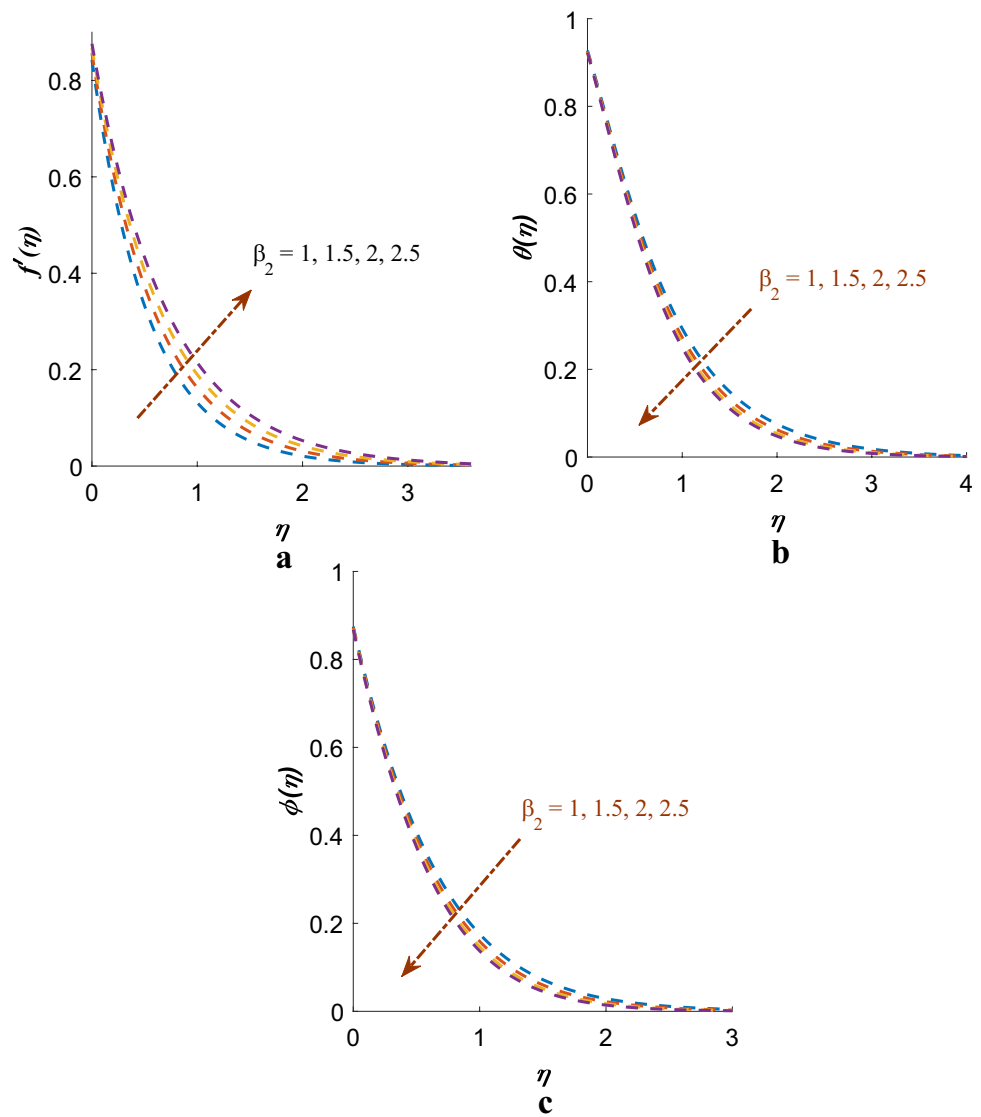
Figure 5. (**a**) Effect of β_2 on $f'(\eta)$. (**b**) Effect of β_2 on $\theta(\eta)$. (**c**) Effect of β_2 on $\phi(\eta)$.
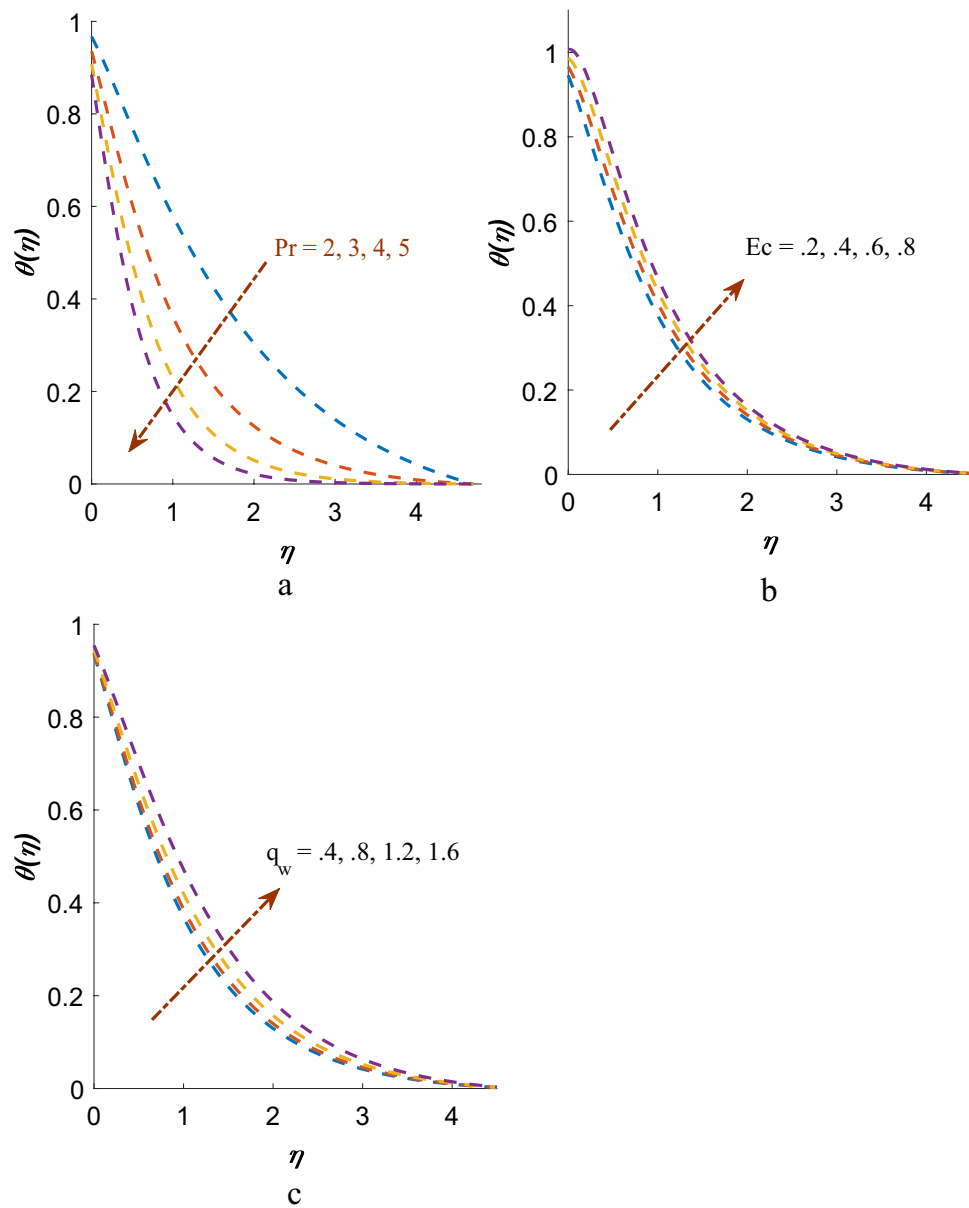
Figure 6. (**a**) Effect of Pr on $\theta(\eta)$. (**b**) Effect of Ec on $\theta(\eta)$. (**c**) Effect of θ_w on $\theta(\eta)$.
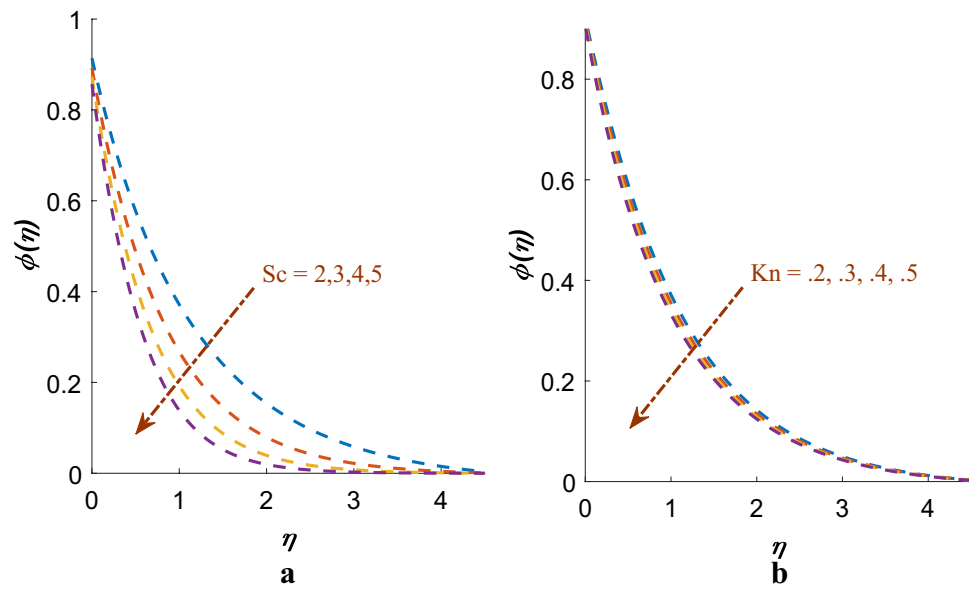
Figure 7. (**a**) Effect of *Sc* on $\phi(\eta)$. (**b**) Effect of *Kn* on $\phi(\eta)$.
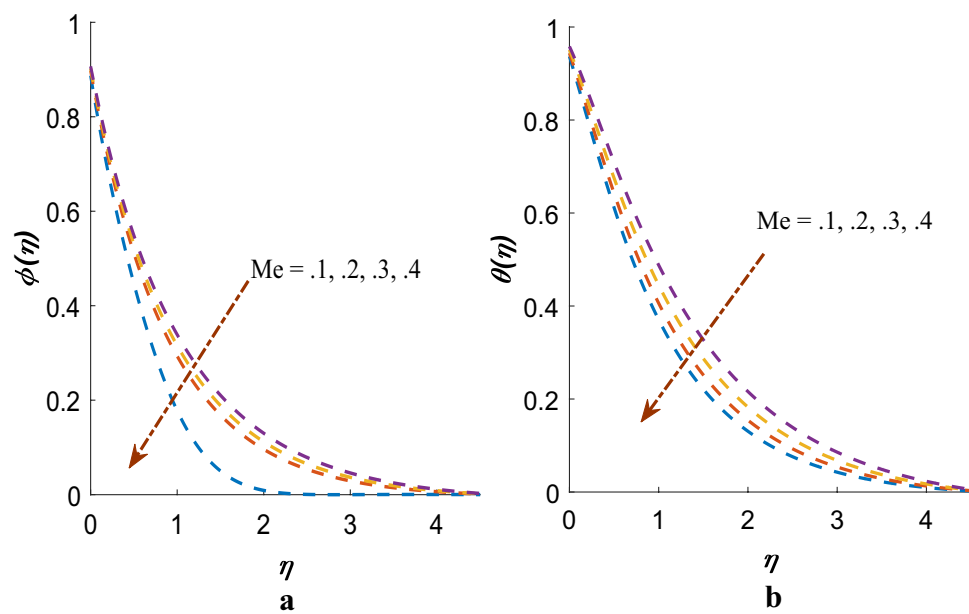
Figure 8. (**a**) Effect of *Me* on $\phi(\eta)$. (**b**) Effect of *Me* on $\theta(\eta)$.
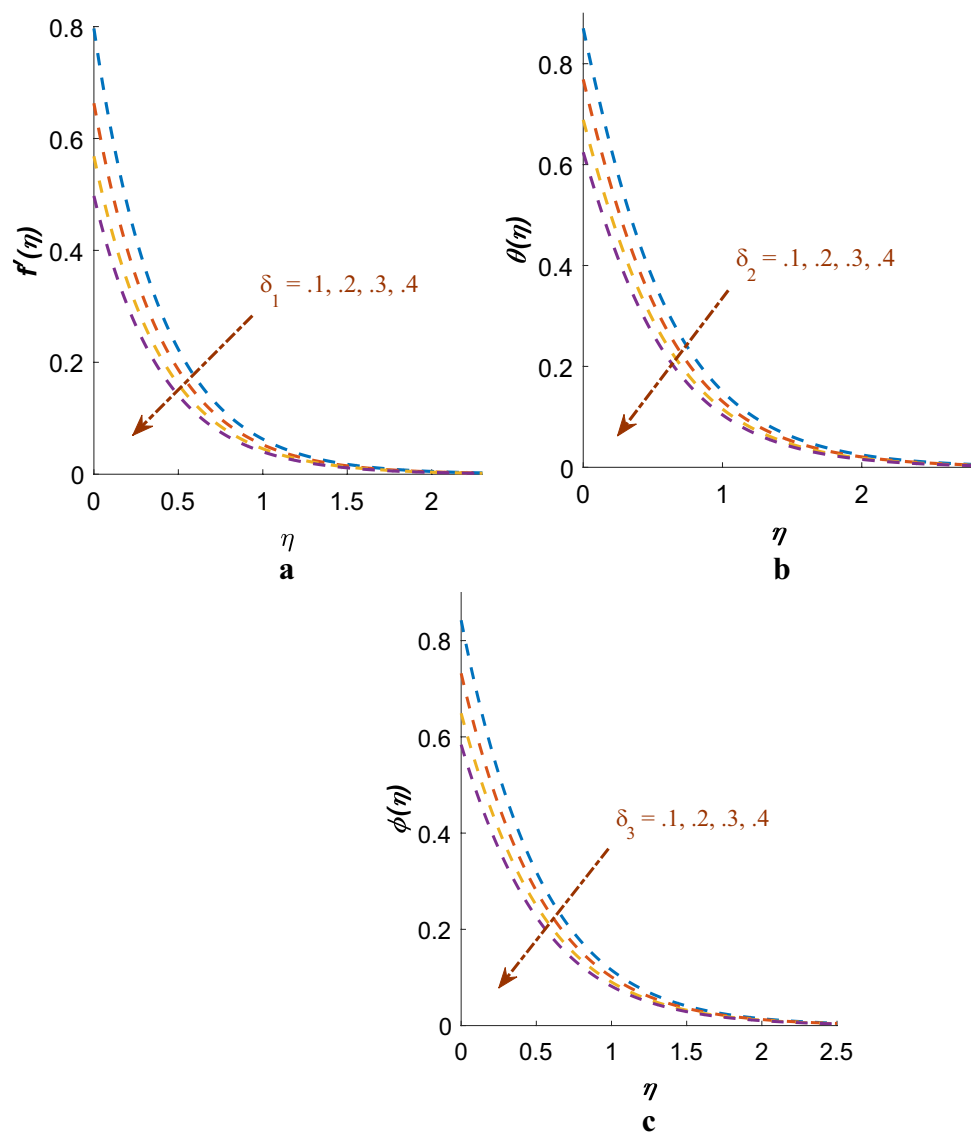
Figure 9. (**a**) Effect of δ_1 on $f'(\eta)$. (**b**) Effect of δ_2 on $\theta(\eta)$. (**c**) Effect of δ_3 on $\phi(\eta)$.
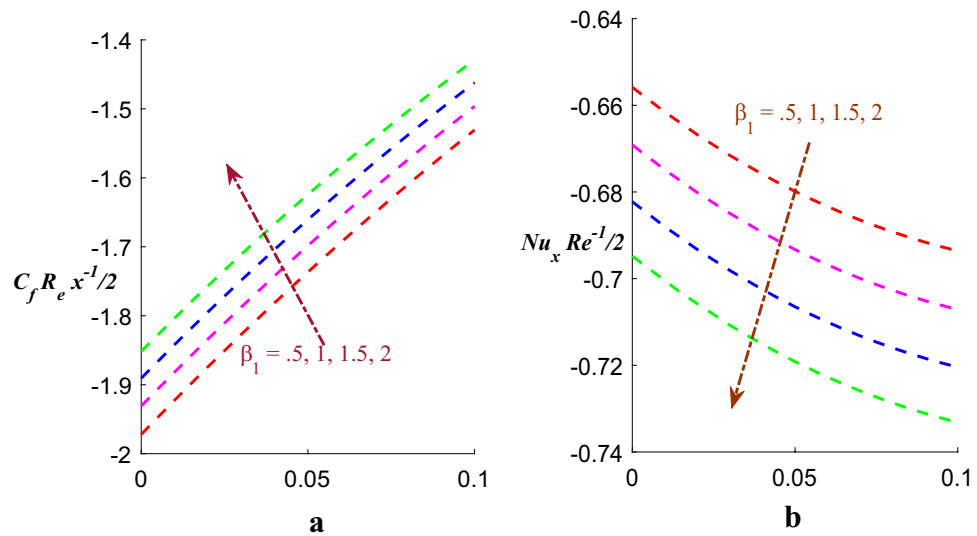
Figure 10. (**a**) Effect of β_1 on Cf. (**b**) Effect of β_1 on Nu.
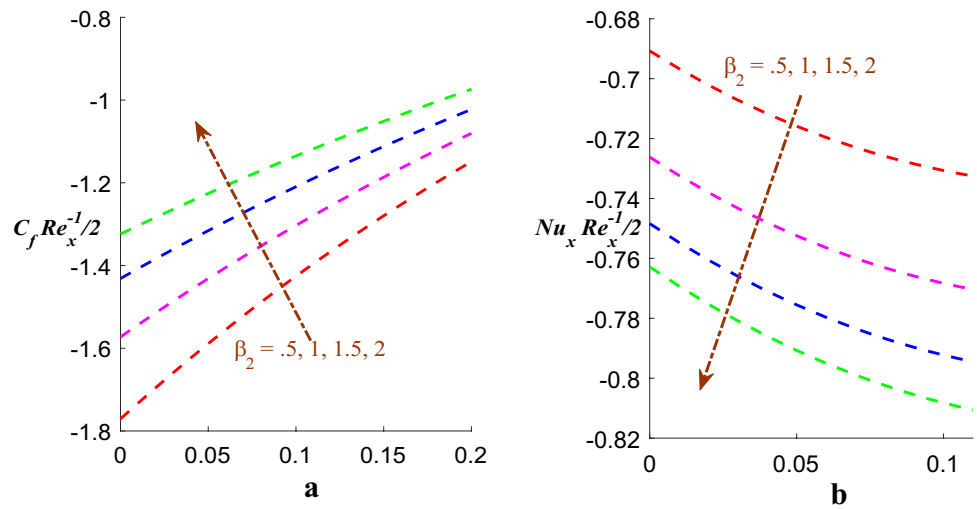
Figure 11. (**a**) Effect of β_2 on Cf. (**b**) Effect of β_2 on Nu.

Data availability

The datasets used and/or analysed during the current study available from the corresponding author on reasonable request.

References

1. Oldroyd, J. G. On the formulation of rheological equations of state. *Proc. R. Soc Lond. Ser. A Math. Phys. Eng. Sci.* **200**, 523–591 (1950).
2. Hayat, T., Shehzad, S. A., Mustafa, M. & Hendi, A. MHD flow of an Oldroyd-B fluid through a porous channel. *Int. J. Chem. React. Eng.*, *10*(1) 1–12 (2012).
3. Fetecau, C., Zierep, J., Bohning, R. & Fetecau, C. On the energetic balance for the flow of an Oldroyd-B fluid due to a flat plate subject to a time-dependent shear stress. *Comput. Math. Appl.* **60**(1), 74–82 (2010).
4. Tan, W. & Masuoka, T. Stokes' first problem for an Oldroyd-B fluid in a porous half space. *Phys. Fluids* **17**(2), 023101 (2005).
5. Goyal, M. & Sharma, S. Investigation of Oldroyd-B fluid flow and heat transfer over a stretching sheet with nonlinear radiation and heat source. *Heat Transf.* **52**, 5361–5380 (2023).
6. Khan, M. N., Nadeem, S., Ullah, N. & Saleem, A. Theoretical treatment of radiative Oldroyd-B nanofluid with microorganism pass an exponentially stretching sheet. *Surf. Interfaces* **21**, 100686 (2020).
7. Olkha, A. & Dadheech, A. Unsteady magnetohydrodynamics slip flow of powell-eyring fluid with microorganisms over an inclined permeable stretching sheet. *J. Nanofluids* **10**(1), 128–145 (2021).

8. Olkha, A. & Dadheech, A. Second law analysis for radiative magnetohydrodynamics slip flow for two different non-Newtonian fluid with heat source. *J. Nanofluids* **10**(3), 447–461 (2021).
9. Dadheech, A., Parmar, A. & Olkha, A. Inclined MHD and radiative Maxwell slip fluid flow and heat transfer due to permeable melting surface with a Non-linear heat source. *Int. J. Appl. Comput. Math.* **7**(3), 89 (2021).
10. Christov, C. I. On frame indifferent formulation of the Maxwell-Cattaneo model of finite-speed heat conduction. *Mech. Res. Commun.* **36**(4), 481–486 (2009).
11. Hosseinzadeh, K. *et al.* Nonlinear thermal radiation and chemical reaction effects on Maxwell fluid flow with convectively heated plate in a porous medium. *Heat Transf. Asian Res.* **48**(2), 744–759 (2019).
12. Gholinia, M., Gholinia, S., Hosseinzadeh, K. & Ganji, D. D. Investigation on ethylene glycol nano fluid flow over a vertical permeable circular cylinder under effect of magnetic field. *Res. Phys.* **9**, 1525–1533 (2018).
13. Khan, M. & Hamid, A. Convective heat transfer during the flow of Williamson nanofluid with thermal radiation and magnetic effects. *Eur. Phys. J. Plus* **134**, 1–12 (2019).
14. Singh, K. & Kumar, M. Melting heat transfer in boundary layer stagnation point flow of MHD micropolar fluid towards a stretching/shrinking Surface. *JJMIE* **8**(6), 403–408 (2014).
15. Hayat, T., Muhammad, K., Alsaedi, A. & Asghar, S. Numerical study for melting heat transfer and homogeneous-heterogeneous reactions in flow involving carbon nanotubes. *Res. Phys.* **8**, 415–421 (2018).
16. Epstein, M. & Cho, D. H. Melting heat transfer in steady laminar flow over a flat plate. *J. Heat Transfer.* **98**(3), 531–533 (1976).
17. Ishak, A., Nazar, R., Bachok, N. & Pop, I. Melting heat transfer in steady laminar flow over a moving surface. *Heat Mass Transf.* **46**, 463–468 (2010).
18. Yacob, A., Ishak, A. & Pop, I. Melting heat transfer in boundary layer stagnation-point flow towards a stretching/shrinking sheet in a micropolar fluid. *Comput. Fluids* **47**, 16–21 (2011).
19. Olkha, A. & Dadheech, A. Second law Analysis for Casson Fluid Flow Over permeable surface embedded in porous medium. *Nonlinear Stud.* **28**(4), 1–13 (2021).
20. Agarwal, K., Baghel, R. S., Parmar, A. & Dadheech, A. Jeffery slip fluid flow with the magnetic dipole effect over a melting or permeable linearly stretching sheet. *Int. J. Appl. Comput. Math.* **10**(1), 1–17 (2024).
21. Dadheech, A., Parmar, A., Agrawal, K., Al-Mdallal, Q. & Sharma, S. Second law analysis for MHD slip flow for Williamson fluid over a vertical plate with Cattaneo-Christov heat flux. *Case Stud. Therm. Eng.* 101931 (2022).
22. Labropulu, F., Husain, I. & Chinichian, M. Stagnation-point flow of the Walters' B'fluid with slip. *Int. J. Math. Math. Sci.* **2004**(61), 3249–3258 (2004).
23. Ali, N., Khan, S. U., Sajid, M. & Abbas, Z. Slip effects in the hydromagnetic flow of a viscoelastic fluid through porous medium over a porous oscillatory stretching sheet. *J. Porous Media* **20**(3), 249–262 (2017).
24. Govindarajan, A., Rajesh, K., Vidhya, M. & Siva, E. P. Effect of mass transfer and slip effect on viscoelastic fluid in a vertical channel with heat source and radiation. In *AIP Conference Proceedings,* vol. 2112(1) 020184 (AIP Publishing LLC, 2019).
25. Dawar, A. *et al.* Analytical simulation for magnetohydrodynamic maxwell fluid flow past an exponentially stretching surface with first-order velocity slip condition. *Coatings* **11**(8), 1009 (2021).
26. Wang, C. Y. Free convection on a vertical stretching surface. *ZAMM-J. Appl. Math. Mech. Z. Angew. Math. Mech.* **69**(11), 418–420 (1989).
27. Andersson, H. I., Hansen, O. R. & Holmedal, B. Diffusion of a chemically reactive species from a stretching sheet. *Int. J. Heat Mass Transf.* **37**(4), 659–664 (1994).
28. Prasad, K. V., Sujatha, A., Vajravelu, K. & Pop, I. MHD flow and heat transfer of a UCM fluid over a stretching surface with variable thermophysical properties. *Meccanica* **47**, 1425–1439 (2012).
29. Khan, W. A. & Pop, I. Boundary-layer flow of a nanofluid past a stretching sheet. *Int. J. Heat Mass Transf* **53**(11–12), 2477–2483 (2010).
30. Sharma, S. *et al.* MHD micro polar fluid flow over a stretching surface with melting and slip effect. *Sci. Rep.* **13**(1), 10715 (2023).
31. Khan, S. U., Majeed, A. & Aziz, S. Thermal prediction of rotatory multiwall carbon nanotubes subject to convective boundary conditions and slip effects: Implicit finite difference simulations. *Numer. Heat Transf. Part B Fundam.* pp. 1–14 (2024).
32. Majeed, A., Zeeshan, A., Ahmad, Q. A. & Ullah, M. Theoretical investigation of Arrhenius activation energy on radiative magneto-hydrodynamic nanofluid flow with heat and mass transfer over a porous cylinder. *Waves Random Complex Media* https://doi.org/10.1080/17455030.2023.2290652 (2023).
33. Majeed, A. & Zeeshan, A. Influence of Brownian motion, thermophoresis and magnetic effects on a fluid containing nanoparticles flowing over a stretchable cylinder. *Fluid Dyn. Mater. Process.* **20**(3), 1–10 (2024).
34. Boujelbene, M. *et al.* Effect of electrostatic force and thermal radiation of viscoelastic nanofluid flow with motile microorganisms surrounded by PST and PHF: Bacillus anthracis in biological applications. *Case Stud. Therm. Eng.* **52**, 103691 (2023).
35. Gari, A. A. *et al.* A thermal case study of three dimensional MHD rotating flow comprising of multi-wall carbon nanotubes (MWCNTs) for sustainable energy systems. *Case Stud. Therm. Eng.* **50**, 103504 (2023).
36. Majeed, A. *et al.* Enhanced thermal and mass transfer of harnessing microbial mediation in electrically conducting Oldroyd-B nanofluid flow: Eukaryotes microorganisms in biological applications. *Case Stud. Therm. Eng.* **51**, 103570 (2023).
37. Li, Y. *et al.* Melting thermal transportation in bioconvection Casson nanofluid flow over a nonlinear surface with motile microorganism: Application in bioprocessing thermal engineering. *Case Stud. Therm. Eng.* **49**, 103285 (2023).
38. Majeed, A., Naeem, S., Zeeshan, A., Qayyum, A. & Alhodaly, M. S. Three-dimensional bio-convection mechanism and heat transportation of nanofluid induced by magnetic field. *Int. J. Modern Phys. B* https://doi.org/10.1142/S0217979224502588 (2023).
39. Fatima, N. *et al.* Three-dimensional analysis of motile-microorganism and heat transportation of viscoelastic nanofluid with nth order chemical reaction subject to variable thermal conductivity. *Case Stud. Therm. Eng.* **45**, 102896 (2023).
40. Majeed, A., Rifaqat, S., Zeeshan, A., Alhodaly, M. S. & Majeed Noori, F. Impact of velocity slip and radiative magnetized Casson nanofluid with chemical reaction towards a nonlinear stretching sheet: Three-stage Lobatto collocation scheme. *Int. J. Modern Phys. B* **37**(09), 2350088 (2023).
41. Majeed, A. *et al.* Analysis of thermal radiation in magneto-hydrodynamic motile gyrotactic micro-organisms flow comprising tiny nanoparticle towards a nonlinear surface with velocity slip. *Alex. Eng. J.* **66**, 543–553 (2023).

Acknowledgements

Author contributions

A.D., Q.A.M. and S.S. conducted the literature review and formulated the problem. A.D. and S.S. carried out the theoretical and numerical analysis. A.D. and Q.A.M. analyzed the results and composed the conclusions. All authors participated in reviewing the manuscript.

Competing interests

The authors declare no competing interests.

Additional information

Correspondence and requests for materials should be addressed to Q.A.-M.

Reprints and permissions information is available at www.nature.com/reprints.

Publisher's note Springer Nature remains neutral with regard to jurisdictional claims in published maps and institutional affiliations.